Electronic Supplementary Material (ESI) for Chemical Communications.

Supporting Information

A novel membrane with heterogeneously functionalized nanocrystal layers performing blood separation and sensing synchronously

Zhenyu Chu, Linlin Li, Gongping Liu, Wanqin Jin*

State Key Laboratory of Materials-Oriented Chemical Engineering, Jiangsu National Synergetic Innovation Center for Advanced Materials, College of Chemical Engineering, Nanjing Tech University, 5 Xinmofan Road, Nanjing 210009 (P.R. China)

*Corresponding auther. E-mail: wqjin@njtech.edu.cn

Materials and Methods

Reagents and apparatuses

Potassium ferrocyanide trihydrate, (Sigma-Aldrich), iron (III) chloride hexahydrate (Sigma-Aldrich), glucose (Sigma-Aldrich), (3-Glycidyloxypropyl) trimethoxysilane (Sigma-Aldrich), sodium L-lactate (Alfa-Aesar), sodium glutamic acid monosodium salt monohydrate (Alfa-Aesar), graphene oxide (GO, JCnano Co., Ltd., China) and 30 wt% H_2O_2 (Sinopharm Chemical Reagent Co., Ltd., China) were used as received. Three enzymes, 84.4 U/mL glucose oxidase (GOx, EC1.1.3.4, 168800 units/g, from Aspergillus niger, Sigma-Aldrich), 2.5 U/mL Lactate oxidase (LOx, EC1.13.12.4, 20 U mg^{-1}, from Pediococcus sp., Sigma-Aldrich) and 0.5 U/mL glutamate oxidase (GMOx, EC1.4.3.11, 5 U mg^{-1}, from Streptomyces sp., Sigma-Aldrich) were immobilized by the 0.2 mg/mL of silane modified GO suspension. The rabbit whole blood was obtained from the mature rabbits (Qinglong animal breeding field, China) by the anticoagulation vacuum blood vessels (EDTA-K2) for the blood cell tests. Specially, for the detection of fibrinogen, the anticoagulation was changed to trisodium citrate. The breeding and the related experiments of the mature rabbits were operated in compliance with the relevant laws and institutional guidelines, and have also approved by the Laboratory Animal Management Committee of Jiangsu Province.

Electrochemical characterizations were conducted by an electrochemical workstation (CHI660C, Shanghai Chenhua, China). All cyclic voltammetry (CV) experiments were operated in PBS at 25 ^oC. A Pt wire and Ag/AgCl were used as the counter and reference electrodes, respectively. The scan rate was 50 $mV \cdot s^{-1}$. Electrochemical Impedance Spectroscopy (EIS) characterization was carried out at the -0.05 V potential. The measurement of the voltage amplitude of 5 mV from the frequency range 0.05 to 10^5 Hz was implemented in a buffer solution. The Scanning Vibrating Electrode Technique (SVET) experiments were performed on PSD-1 (Applicable Electronics, LLC., USA). All field emission scanning electron microscopy (FESEM) images were taken on Hitachi-4800. Atomic force microscopy (AFM) was applied using the XE100. The glucose level in blood was analyzed by a glucometer (ACCU-CHEK@Performa, Roche Diagnostics GmbH, Germany) to calibrate the results obtained by the as-prepared device. A sterilizer (SN510C, YAMATO, Japan) was introduced to fulfill the sterilization treatment of hollow fiber support, the PB deposited hollow fiber and all modules and components for the enzyme loading at the temperature of 121 ^oC.

Methods:

Membrane fabrication

Aluminum ceramic hollow fiber precursors were prepared by spinning a suspension of a polymer solution (polyethersulfone, N-methyl-2-pyrrolidone and polyvinyl pyrrolidone) and alumina powders. The finger-like and sponge structures in these hollow fiber membranes can be adjusted by controlling the solvent-nonsolvent exchange rate. PB was synthesized using a vacuum self-assembly approach to form 40 deposition layers on the surface and inner channels of hollow fibers (Supplementary Fig. 2). The direction of the driving force was from the outer to the inner surface for membrane preparation.

Measurements of sensing membrane and its device

The interfacial adhesion strength of the PB membrane was measured by the nano-indentation technique. A conical indenter was used to scratch with a 60º angle, 5 μm radius and 20 μm

polished depth. Dynamic load, penetration depth, and friction force were monitored and recorded by the sensing probe. The scratch of the PB membrane was then magnified by FESEM and analyzed with the recording data of nano-indentation. The SVET technique was used to characterize the current channel of the PB membrane. A PB membrane with 0.1 mm effective height was fixed on the anti-vibration platform, and immersed in the 0.1 M KCl solution. The microelectrode diameter was approximately 1 μm. The tip of the electrode was platinized to increase the surface area to 10 μm. The vibration frequency was set to 80 Hz in a perpendicular direction to the surface. The current density changes of the PB membrane cross section were recorded at different times. The as-designed device shown in Fig. 1a was used for all electrochemical and separation characterizations. The vacuum pressure applied to the inner tube of the PB membrane was kept at 0.09 MPa. The CV signal acquisition began when the electrolyte had filled all channels, and was collected at a 0.1 V/s scanning rate. Fresh rabbit whole blood with anti-coagulation treatment was used for the synchronous separation and sensing experiment. The PB membrane, platinum and silver wires were respectively integrated to serve as work, counter and reference electrodes. When working, three electrodes were connected to the electrochemical station, and the evacuation was imposed on the PB membrane. The chronoamperometry method was used to in-situ monitor the electrochemical signal during the whole process. The analysis was performed at the time of formation of a stable current. Then, the target index of blood was detected by CV scanning in reference to the former linear calibration. The concentrations of blood cells were examined by an automatic hematology analyzer, and the content of fibrinogen was measured by a coagulometer. The fresh whole blood and collected serum were both analyzed and compared to evaluate the separation performance of the as-prepared device.

Supplementary Figures

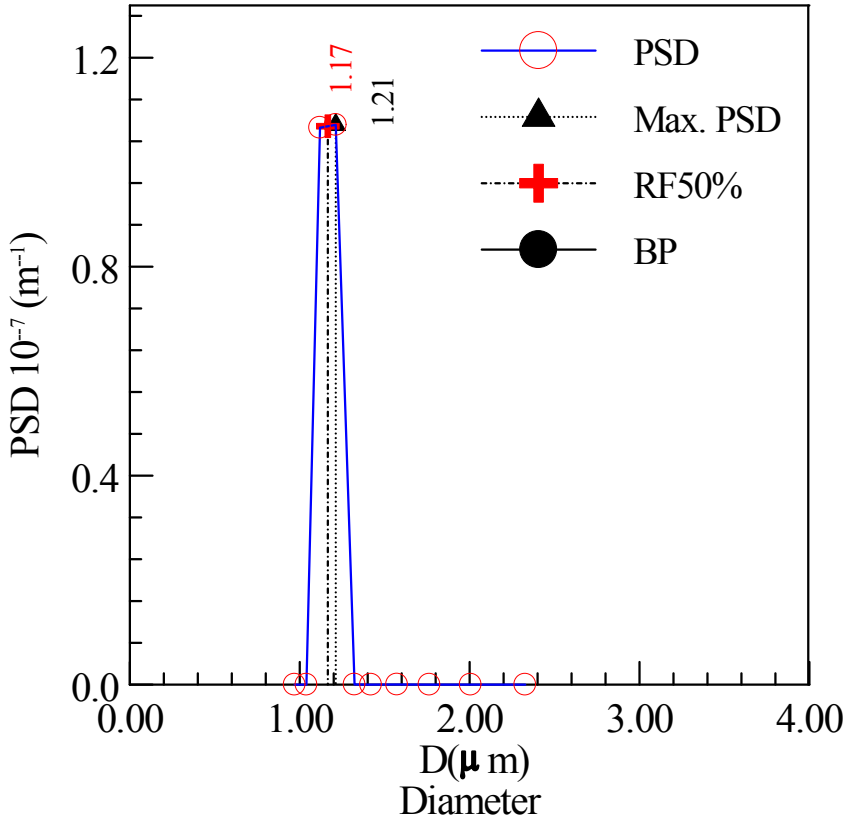

Fig. S1. Pore size distribution of Al_2O_3 hollow fiber by bubble pressure test.

A 6 cm Al_2O_3 hollow fiber was one-end sealed for bubble pressure characterization. The test pressure was continuously increased to push the bubble generation through the hollow fiber pores. The bubbling point under the 0.042 L/h N_2 flow was determined to be 0.045 MPa, indicating the biggest pore size of 6.46 μm according to the Laplace equation[1]:

$$\Delta P = 2\gamma/r \qquad \text{Eq. 1}$$

Where ΔP is the applied pressure to membrane, $\gamma$the surface tension, and r the pore radius.The collected data were analyzed to plot the pore size distribution as shown in Supplementary Figure 1. The average size of hollow fiber was as large as 1.17 μm. Therefore, bare Al_2O_3 HF was not suitable for direct separation of serum. The whole pore size is much larger than fibrinogen, even than platelet. Furthermore, the desire HF with a smaller pore size suitable for serum collection can only be obtained by increasing the calcination to 1400 °C, along with an energy-intensive fabrication and a significant loss of membrane flux.

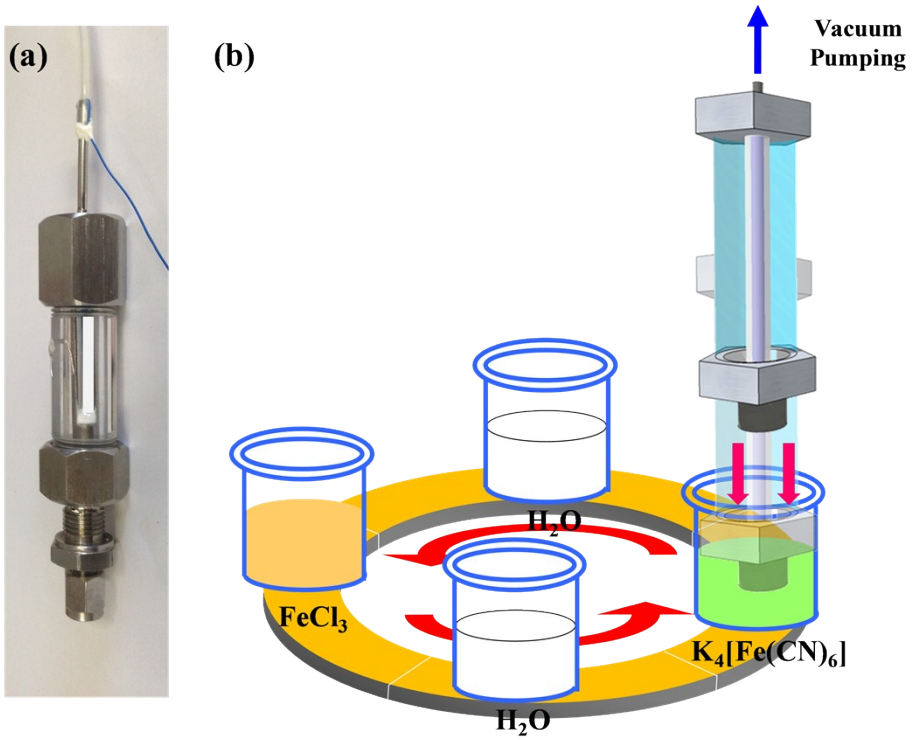

Fig. S2. (a) Stainless steel PB membrane deposition module, and (b) scheme of PB membrane preparation by a vacuum self-assembly approach.

It was expected that PB would not only cover the outer surface of hollow fiber, but also penetrate into the cavities to facilitate the sensing function. Therefore, as shown in Fig. S2a, a customized module was fabricated to enable the channel self-assembly of PB membrane for the novel separation-sensing integration. A clean Al_2O_3 hollow fiber was first introduced into the module, and then the module exit was sealed to expose only one end. A 0.09 MPa vacuum pressure was imposed to suck the reactive solution. For the self-assembly process, two solutions were prepared for PB membrane preparation. Solution 1 (S1): 0.01 M $K_4[Fe(CN)_6]$ + 0.1 M KCl + 0.1 M HCl. Solution 2 (S2): 0.01 M $FeCl_3$ + 0.1 M KCl + 0.1 M HCl. The preparation route is schematically shown in Suppl. Fig. 2b. The module was first dipped into S1 for 60 s, and then transferred into the deionized water for three times with each duration of 15 s to rinse away the excessively adsorbed reactants. Subsequently, S2 solution was introduced to react with former $K_4[Fe(CN)_6]$ by adsorption, followed by the same washing procedure using deionized water. One layer of PB would be deposited after above self-assembly process was completed once. Normally, several tens of layers were required for regular growth of PB crystals.

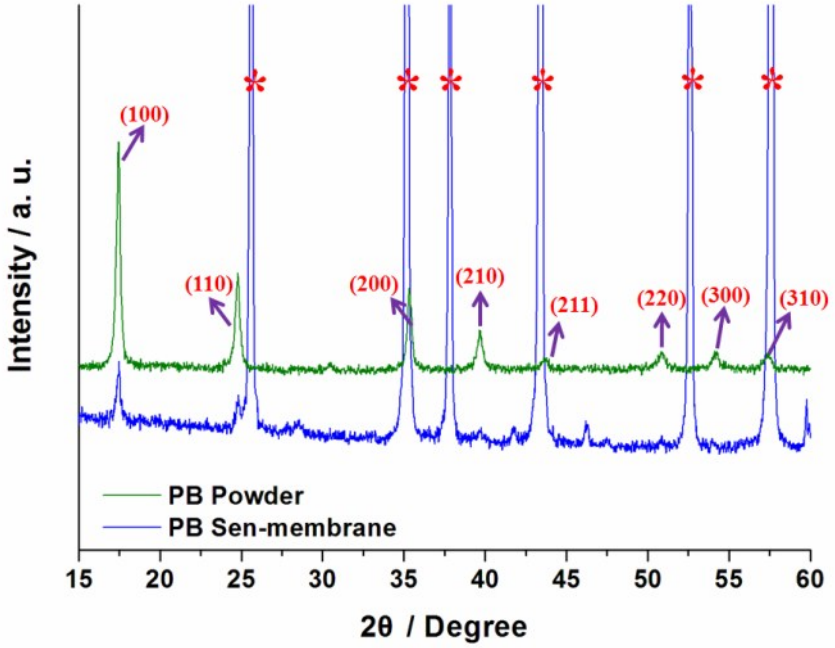

Fig. S3. XRD patterns of pure PB powders and the prepared PB sen-membrane (*: the characteristic peaks of Al_2O_3).

XRD patterns of both pure PB powders and the powders of grinded PB sen-membrane were obtained to check if the PB layers were successfully deposited on Al_2O_3 surface. Fig. S3 shows that the characteristic peaks of PB were clearly observed in the pattern of grinded powders of the as-prepared sen-membrane. This can strongly confirm that the Al_2O_3 hollow fiber can support the sufficient crystallization of PB.

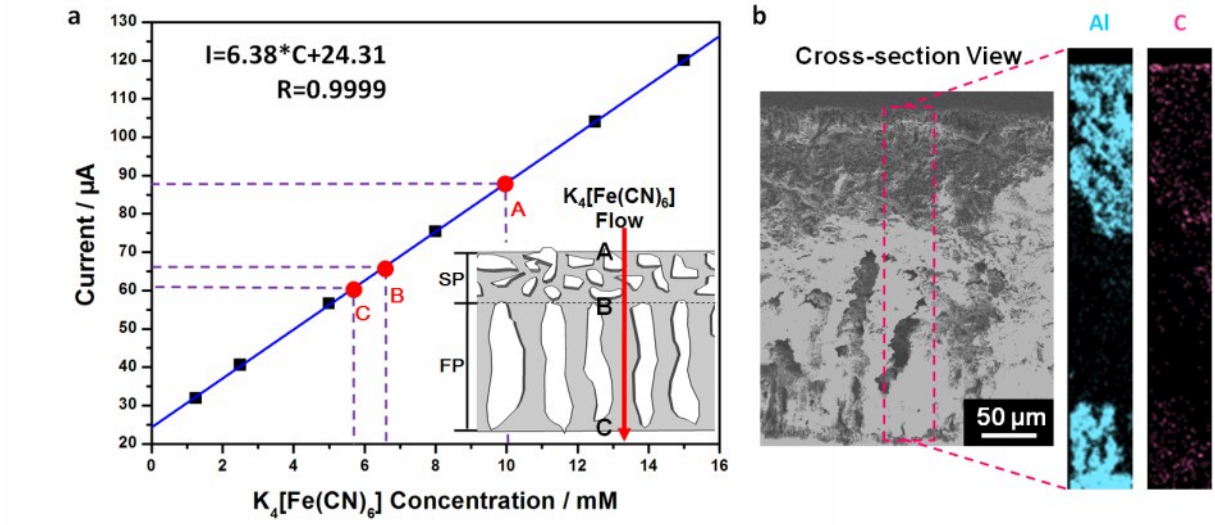

Fig. S4 (a) Calibration curve of the response current vs. $K_4[Fe(CN)_6]$ concentration drawn by CV technique. Points A to C represent the $K_4[Fe(CN)_6]$ solutions collected at the outer surface, the joint between SP and FP, and the inner surface of hollow fiber, respectively. (b) EDS analysis of Al and C elements of the as-prepared PB sensing membrane.

The growth mechanism of the PB nano-crystal was further investigated based on its crystallization behavior. The $K_4[Fe(CN)_6]$ solution served as the first reactant for the PB seed growth. The concentrations of unabsorbed $K_4[Fe(CN)_6]$ at different sections of the support were monitored during the preparation. CV calibration (Fig. S4a) confirmed that the adsorption at the SP layer was stronger than that at the FP layer, as indicated by the evident decrease of residual $K_4[Fe(CN)_6]$ concentration. The EDS results also showed that the amount of PB formed, which was delegated by the C element, was higher in the SP region accompanied with a high Al_2O_3 content.

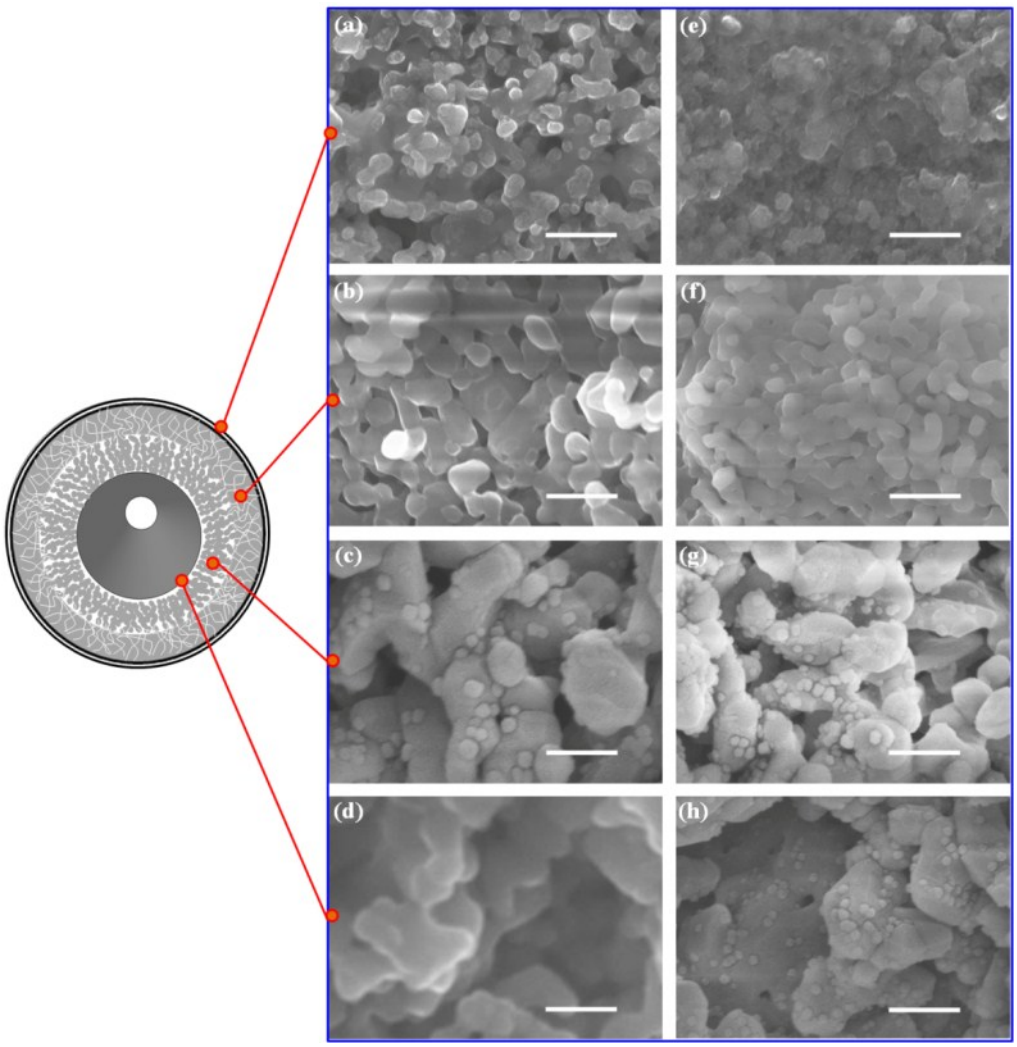

Fig. S5. FESEM images of different parts of PB membrane with 20 (a - d) and 30 (e - h) self-assembled layers. Scale bar: 1.5 μm.

The growth mechanism can be characterized by monitoring the structure evolution with different self-assembled layers. For outer surface of tuber with 20 layers, isolated PB particles covered the whole Al_2O_3 surface, but there were still lots of holes that were not fully filled. Till 30 layers, it could hardly observe the single PB particle. All PB crystals appeared intergrowth to eliminate the big holes. It was shown that in sponge pore region, 20 layers can also cause the mutual stacking of PB crystals to form the basic PB layer, but rare big crystals grow on it. Ten more assembly layers can produce much smaller crystals which were close to cubic structure. Compared with the PB structures in finger layer, after 30 layers assembly, the crystal size was reduced to almost half compared to that of 20 layers. But at the site of inner surface, no PB formed on Al_2O_3 surface for 20 layers due to the low concentration of reactive solution. Analysis of above growth evolution, we can find that the different support structure will strongly affect the morphology of produced PB. Meanwhile, sufficient self-assembly steps would also determine of PB crystallization.

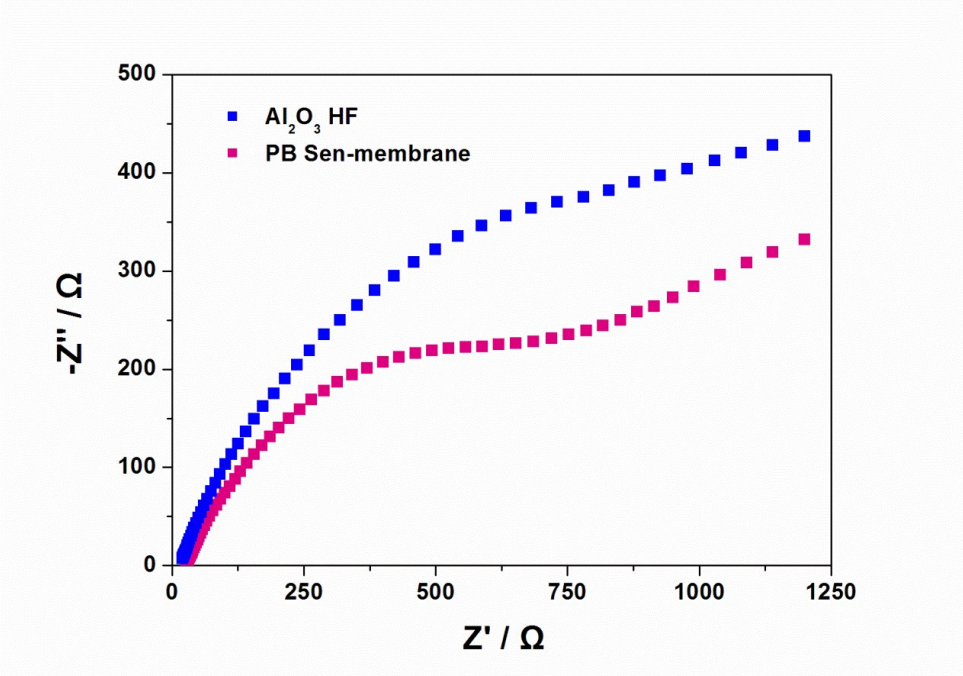

Fig. S6. EIS results of Al_2O_3 HF and the prepared PB sen-membrane under the cavities filled by a buffer solution.

In general Al_2O_3 is can be regarded as an insulator with very poor conductivity[2], while Prussian blue is a semiconductor[3]. For electrochemical analysis of physiological substances, conductivity is an important parameter for catalytic electrons transportation. Accordingly, EIS experiments were operated to compare the electron transfer resistances between Al_2O_3 HF and PB membrane under the electrolyte surrounding. The values of electron transfer resistances were 1457.62 and 963.22 Ω for Al_2O_3 HF and PB membrane respectively. The results indicated that the deposition of PB layer into the cavities of HF can significantly improve the electron transfer rate with the electrolyte.

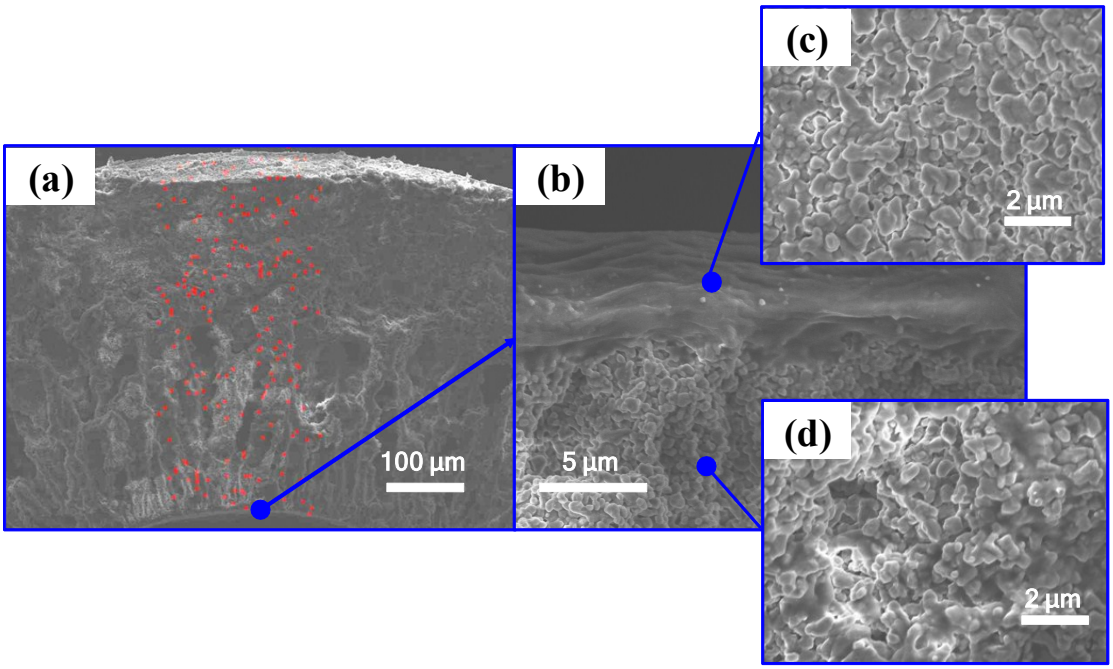

Fig. S7. FESEM images of enzyme loaded PB membrane: (a) general view, the red spots represent S element distribution which came from graphene oxide linked enzyme by EDX characterization; (b) cross-section view of inner tuber; (c) inner surface; and (d) finger pore layer surface.

Glucose oxidase was immobilized by vacuum pump across inner to outer surfaces of the sen-membrane to complete the sensing ability to blood sugar. It was noted that the loaded enzyme would not block all the pores of inner surface, otherwise, the separation resistance would be tremendously increased to hinder the driving force for serum collection. Thereafter, S element of graphene oxide/enzyme was employed as the marker to investigate the enzyme distribution in PB membrane decorated hollow fiber. As shown in Fig. S7a, S can be detected from all the inner to outer profiles indicating that enzyme was immobilized into the channels instead of the surface only. The inner surface can form a layered film, which was attributed to the introduction of graphene oxide as the enzyme linker. However, according to the image of Fig. S10c, this layer did not block all surface pores. There were still lots of pores bigger than 100 nm appeared on the surface which could guarantee the fast transfer of the separated serum. The finger pore surface that served as the main sensing component was already sufficiently covered by a layer of enzyme for readily detection.

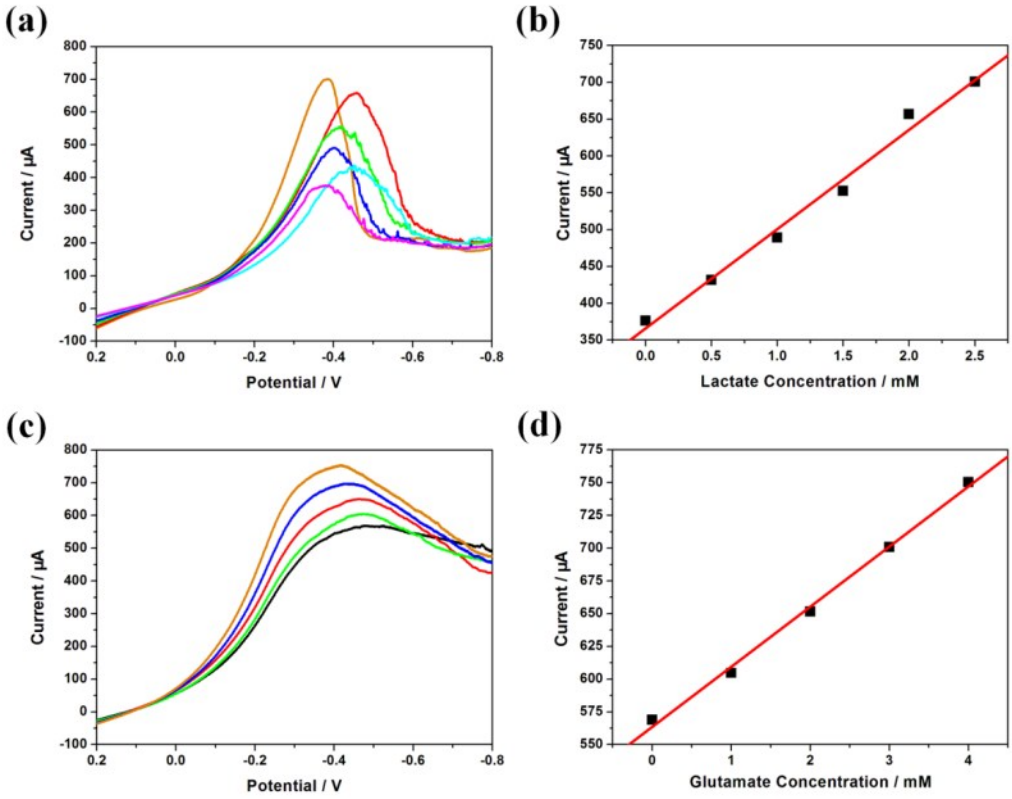

Fig. S8. CV characterizations of the designed device for the detections of lactate (a) and glutamate (c). (b) and (d) were respective linear calibrations of lactate and glutamate detections.

The sensing function of PB is dependent on the electrocatalysis of H_2O_2 from the oxidase reactions. Thus, this gives the versatile detection capacities by the immobilization of different oxidases. Blood sugar detection is related to diagnose the diabetes. Moreover, blood lactate and glutamate are also essential indexes for health indication. Lactate index often reflects the hypoxia, poor perfusion of tissue, acute circulatory shock, liver failure, congestive heart failure and diabetic ketoacidosis, etc. Glutamate unbalance can indicate the nerve and liver diseases. Therefore, lactate and glutamate oxidases were respectively immobilized to enable the versatile detections of L-lactate and L-glutamate. As shown in Fig. S8, with the increase of L-lactate and L-glutamate concentrations, the peak values of reduction current also proportionally increase. The sensitivities of lactate and glutamate oxidases modified PB sen-membranes were 134.92 and 45.90 $\mu A \cdot mM^{-1}$ demonstrating the promising analysis of blood lactate and glutamate.

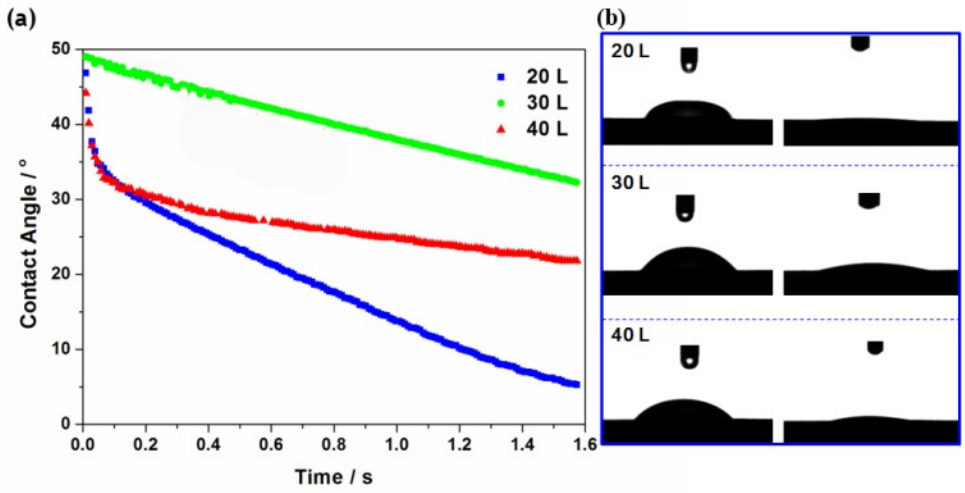

Fig. S9. Dynamic contact angle characterizations of PB membrane with 20, 30 and 40 layers: (a) effect of layer numbers on the contact angle; (b) digital photos of drop on membrane surface at 0 and 1.6 s.

A heavy problem in blood separation is the membrane pollution due to the high viscosity caused by blood cells and proteins. The cells were much bigger than membrane pores so they might easily accumulate on the surface to block the separation channels. Therefore, a hydrophilic surface was required to hinder the cells deposition and accumulation on the membrane surface. To this end, the as-prepared PB membranes with different assembly layers were tested by dynamic contact angle experiments. The results showed that at the contact angles were 46.9, 49.0 and 44.2 degrees for 20, 30 and 40 layers, respectively. This can indicate the hydrophilic nature of PB membrane surface. Within very short time, water drop will immediately permeate into cavities to exhibit the continuous decrease of angle degrees. Among three membranes, 20 layers PB possessed the fastest permeation which is attributed to the fewest coverage to expose the biggest hole size. PB membrane prepared by 40 layers own the lowest contact angle to exhibit best hydrophilic surface avoiding of membrane pollution.

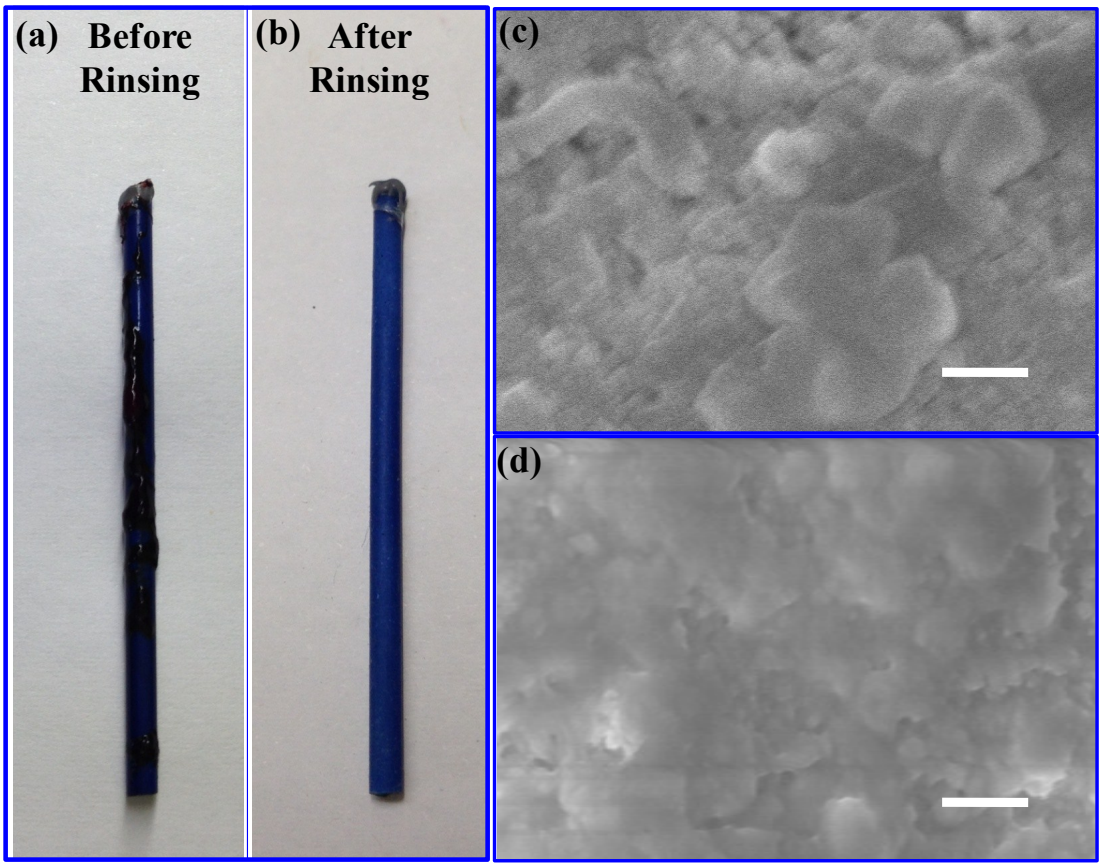

Fig. S10. Digital photos of used PB membrane before (a) or after (b) rinsing by water, the fresh (c) and the used PB membrane (d). Scale bar: 300 nm.

The used PB membrane shown in Fig. S10a was partially covered by coagulated blood cells. But this pollution can be easily cleaned up by water rinsing. Furthermore, as evidenced by the FESEM images, after rinsing the surface was not shielded. Pores can be still observed to confirm the benefit of hydrophilic surface for pollution reduction.

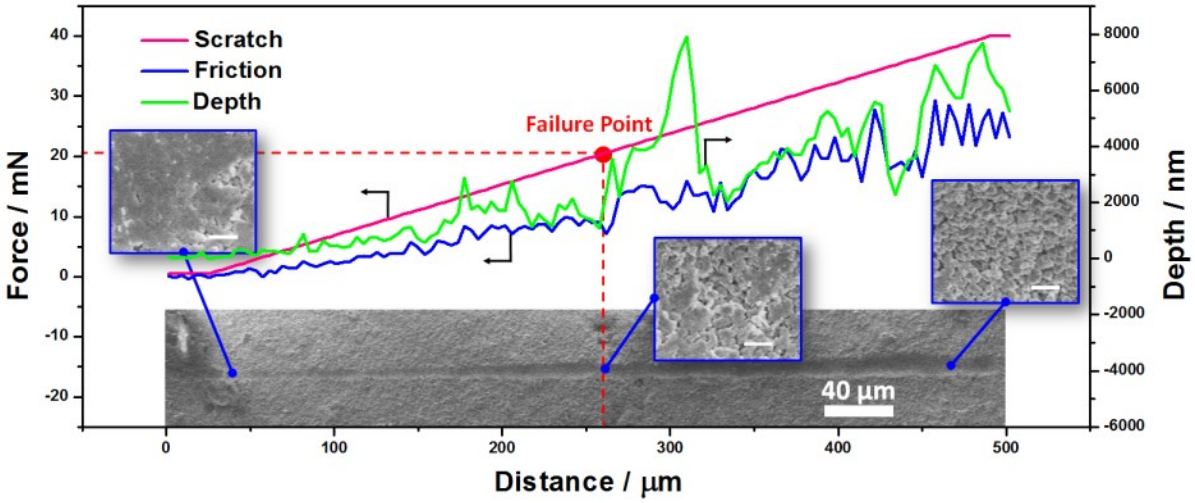

Fig. S11. Nano-indentation characterization of PB sensing membrane for mechanical strength investigation. Insets show the FESEM images of different scratch sites. Bar = 1 μm.

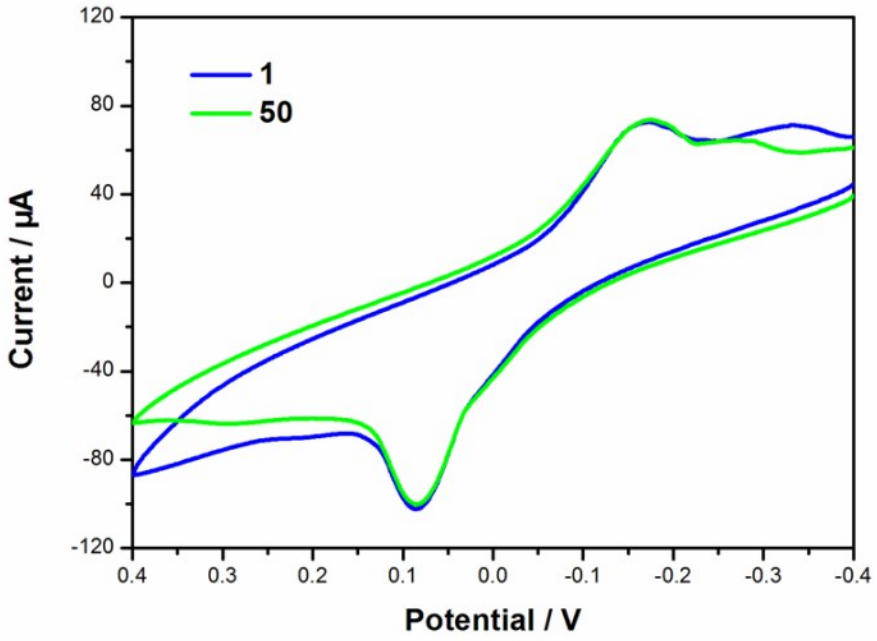

Fig. S12. CV curves of the PB membrane at the first and the 50th tests.

Due to the application in blood analysis, during the electrochemical detection, PB membrane needs to firmly attach on the Al_2O_3 HF. CV repeated tests can be applied to investigate the maximum redox electron amount which is directly related to PB coverage[4]. After the 50 times scanning, the redox peaks just showed very slight change confirming that the prepared PB membrane possessed an excellent electrochemical stability owing to the strong interaction between CN group and Al_2O_3 support.

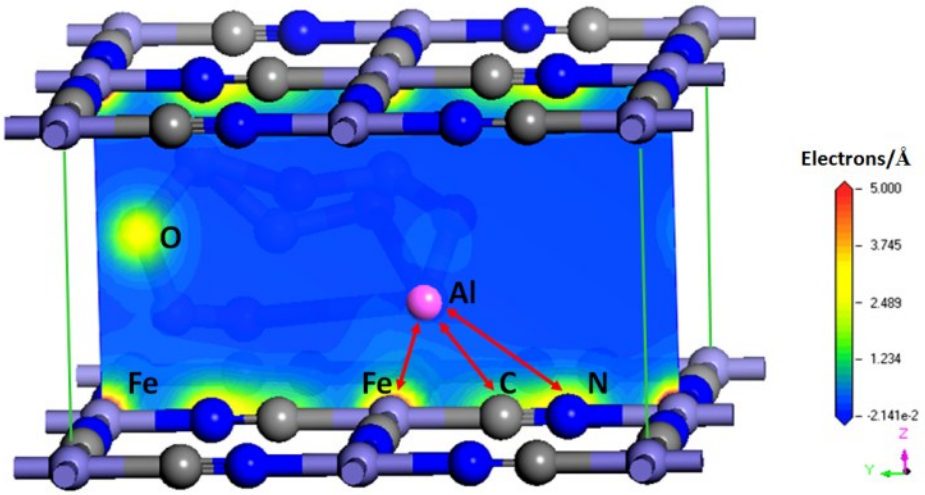

Fig. S13. Electron cloud distribution of PB adsorbed Al_2O_3 model.

For investigation of the interactions between PB and Al_2O_3, DFT was applied to simulate the adsorption behavior between PB and Al_2O_3. First, a representative model was established as follows:

1. PB face-centered cubic and α-Al_2O_3 unit cells were respectively built and simulated by geometry optimization.
2. The (001) crystal face of PB was cut and 10 Å vacuum layer was added between neighboring facet to provide the reaction space.
3. A typical Al_2O_3 repetitive unit was placed into the vacuum layer as the adsorption model, and then DFT simulation was executed.

Perdew Burke Ernzerhof was selected as exchange-correlation functional Convergence tolerance setting: (1) energy tolerance was 2×10^{-5} eV/atom; (2) maximum force, stress and displacement was set as 0.05 eV/ Å, 0.1 GPa and 0.002 Å, respectively. The energy cutoff was adjusted to be 300 eV for reaching convergence.

Electron cloud was applied to visualize the possible movement track of the electrons. Normally, the interaction formation was also accompanied with the overlap of electron cloud[5,6]. As shown in Fig. S13, the Al atom from Al_2O_3 demonstrates overlap with C, N and Fe atoms suggesting the bonding possibility. Moreover, electrons of Fe were attracted to induce the change density feature by Al atom. This may illustrate the loss of electron and valance increase of Fe. On the contrary, the original densities of CN group did not change much after the function of Al_2O_3. But there was a mutual electron region between CN and Al. The confirmation of interactions between Al and CN should be further investigated by experiments.

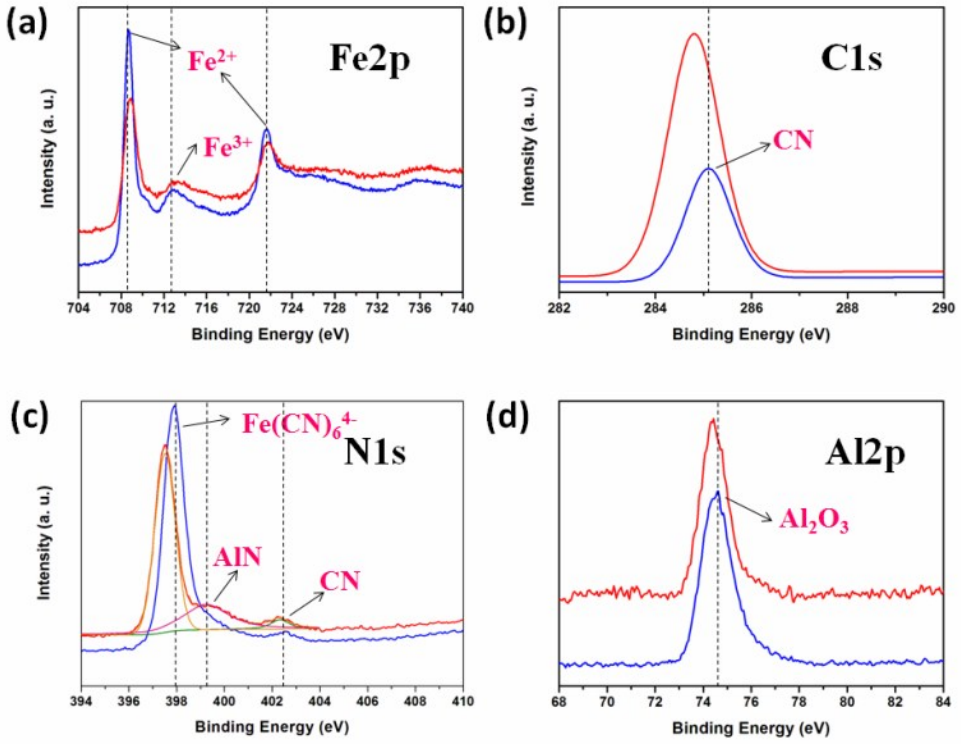

Fig. S14. XPS spectra of PB membrane compared with those of pure PB or Al_2O_3 powders. Blue lines represented the pure powders' elements, and red lines were PB membrane results.

The theoretical studies based on DFT showed that the interaction between PB and Al_2O_3 mainly come from Al, Fe, C and N elements. Therefore, XPS spectra of these elements were obtained for experimental studies. For comparison, the XPS spectra of pure PB powders and Al_2O_3 powders grinded from hollow fiber were also acquired. As shown in Fig. S14a, the two typical peaks[7] of Fe2p changed from 708.6 and 721.5 eV to 708.8 and 721.8 eV, respectively. In the unit cell of PB, Fe^{2+} is close to C atom which possesses a weaker electronegativity than N atom. The low energy shift indicated the escape of electrons, which was consistent with the DFT results. Both C and N from CN group[8] shifted to low binding energies with around 0.3 and 0.4 eV, respectively. More importantly, a new peak appeared in the N1s spectrum at 399.2 eV which was ascribed to AlN[9] interaction. The emerging XPS signal can firmly indicate that the deposition of PB on Al_2O_3 surface was mainly relied on the chemical combination between N and Al, along with the weak interaction of other atoms. The strong bonding would be beneficial for the stability of PB membrane.

Supplementary Video

This video shows the on-line separation and sensing process for the rabbit whole blood. The driving force for separation was 0.09 MPa vacuum pressure by a pump. Meanwhile, the membrane, counter and reference electrodes were connected to the electrochemical workstation. CV scanning was continuously operated to the device for recording the biosensing signals of the blood sugar.

Supplementary references

1. D. Shin, et al, Growth dynamics and gas transport mechanism of nanobubbles in graphene liquid cells, *Nat. Commun.* **2015**, *6*, 6068.
2. A. Jiang, et al. The inlaid Al_2O_3 tunnel switch for ultrathin ferroelectric films, *Adv. Mater.* **2009**, *21*, 2870-2875.
3. D. Gimenez-Romero, et al. Evidence of magnetoresistance in the Prussian blue lattice during a voltammetric scan, *J. Phys. Chem. C* **2008**, *112*, 20099-20104.
4. Y. Liu, Z. Chu, W. Jin, A sensitivity-controlled hydrogen peroxide sensor based on self-assembled Prussian Blue modified electrode, *Electrochem. Commun.* **2009**, *11*, 484-487.
5. K. Leung, et al., Density functional theory and DFT+U study of transition metal porphines adsorbed on Au(111) surfaces and effects of applied electric fields, *J. Am. Soc. Chem.* **2006**, *128*, 3659-3668.
6. A. Botello-Mendez, et al, Achievement of DFT for the investigation of graphene-related nanostructures, *Acc. Chem. Res.* **2014**, *47*, 3292-3300.
7. A. Omura, et al. Electrochemical control of the elution property of Prussian blue nanoparticle thin films: mechanism and applications, *Phys. Chem. Chem. Phys.* **2009**, *11*, 10500-10505.
8. L. Zhang, et al. Biosensor based on Prussian blue nanocubes/reduced graphene oxide nanocomposite for detection of organophosphorus pesticides, *Nanoscale* **2012**, *4*, 4674-4679.
9. H. Liao, R. Sodhi, T. Coyle, Surface composition of AlN powders studied by x-ray photoelectron spectroscopy and bremsstrahlung-excited Auger electron spectroscopy, *J. Vac. Sci. Technol. A* **1993**, *11*, 2681-2686.